Astron. Astrophys. 300, 791–807 (1995)

ASTRONOMY AND ASTROPHYSICS

On the collimation of stellar magnetospheres to jets

I. Relativistic force–free 2D equilibrium

C. Fendt[1,2], M. Camenzind[2], and S. Appl[2]

[1] Lund Observatory, Box 43, S-22100 Lund, Sweden
[2] Landessternwarte Königstuhl, D-69117 Heidelberg, Germany

Received 7 July 1994 / Accepted 16 October 1994

Abstract. Protostellar jets are most probably disk winds or stellar winds collimated by rotating magnetospheres. The structure of these magnetospheres follows from solutions of the Grad–Schlüter–Shafranov (GSS) equation for the force–balance between axisymmetric magnetic surfaces. In this paper, two–dimensional force–free solutions of the relativistic GSS equation are numerically obtained for different field topologies of the underlying magnetosphere. Due to the high rotational periods observed for T Tauri stars, the light cylinder of rotating protostellar magnetospheres is within the observed jet radii. This requires a special relativistic treatment of the GSS equation, which is solved using the method of finite elements. In this approach, boundary conditions along the Alfvén surface are automatically satisfied. The code enables the solution of the GSS equation in the entire domain between the stellar surface and the asymptotic jet region.

The magnetosphere which carries the plasma flow is assumed to be generated by the central star. For stellar field strengths of the order of a kilo–Gauss, a gap between the stellar surface and the inner edge of the accretion disk opens up. Two different magnetic field topologies are considered depending on the behaviour of the magnetic fields near the inner accretion disk. In the case of accretion disks with high resistivity, a reversed field topology is built up along the accretion disk, and the current exchange between star and disk mainly flows in the inner magnetosphere. This is consistent with high mass–accretion along the dipolar stellar fields and small mass loss rates through the wind.

In the case of accretion disks with low resistivity, a screw pinch topology results, since the accretion disk screens the magnetosphere of the star. Smooth field topologies can be calculated in this case which are collimated into asymptotic cylinders with radii of a few light cylinder radii. In general, such solutions are found to have kinks along the Alfvén surface. For a proper adjustment of the underlying current distribution and the shape of the jet boundary, one can find magnetic field configurations without kinks at the Alfvén surface. In this case, plasma flows smoothly through the Alfvén surface. The distribution of the wind plasma is calculated from particular solutions of the wind equation.

The paper mainly concentrates on protostellar jets since the stellar jet phenomenon is predominantly observed for young stellar objects. The results, however, are also applicable for other astronomical jets emerging from star–disk systems. In particular, the problem of magnetic fields with kinks at the light cylinder is well known in the context of pulsar magnetospheres. Our results provide a solution to this longstanding problem.

Key words: magnetohydrodynamics – ISM: jets and outflows – stars: pre-main-sequence – stars: magnetic field – stars: mass loss – pulsars: general

1. Introduction to jet formation

Observations show that young stellar objects may consist of three main components: A protostellar object (a T Tauri star (TTS) or an IR protostar), an accretion disk and, occasionally, bipolar outflows in the form of highly collimated high velocity jets or weakly collimated low velocity molecular flows and winds (Appenzeller & Mundt 1989; Bertout 1989; Camenzind 1990, hereafter CA; Montmerle et al. 1993). In addition, there is strong evidence that magnetic fields play an important or even the dominant role in the evolution and interaction of these components.

VLA and VLBI radio observations suggest that these stars have a dipolar kG magnetic field (André et al. 1988, 1991). The magnetic structure of the stellar surface is also plausible from measurements of rotational periods of TTSs: Cold and hot spots or flares on the surface lead to photometric variations (Bouvier et al. 1993). This method, however, gives only upper limits for the magnetic field strength ($\lesssim 1$ kG).

The orientation of the bipolar outflows in star forming regions is found to be mainly parallel to the ambient magnetic

Send offprint requests to: C. Fendt (Lund Observatory)

field direction (Appenzeller & Mundt 1989; Reipurth 1989). As suggested by Mundt et al. (1990), a magnetic current carrying jet would be able to explain the observed jet bending due to the cloud field in the HL Tauri region. Bow shock observations give estimates of the pre–shock jets magnetic field strength of the order of 10 μG (Morse et al. 1992, 1993).

The relatively low rotational periods of TTSs can be explained by a magnetic link between the magnetic star, the accretion disk and the escaping wind. The field removes angular momentum from the star and transfers it to the disk and the jet. Thus, the star can be decelerated efficiently on time scales comparable to its age (CA, Königl 1991). Further, there is an observational correlation between the detection of accretion disks and bipolar outflows: Contrary to classical TTSs, the subclass of naked TTSs shows neither the signature for the existence of an accretion disk nor hints to bipolar outflows or jets. A physical model therefore has to explain simultaneously both accretion and wind phenomena. Whether classical TTSs and weak line TTSs are different stages of the same stellar evolutionary track or follow different tracks is still an open question.

The first theoretical treatment of the scenario of magnetized disk winds was given by fundamental papers of Blandford & Payne (1982) and Pudritz & Norman (1983). However, for solving the GSS equation they assumed self–similarity (BP) or another special scaling (PN) which both imply e.g. an infinite jet radius. Sakurai investigated the GSS equation for a stellar wind (1985) as well as for a disk wind topology (1987) and showed that field lines of an initial monopole type geometry will bend towards the rotational axis.

Camenzind (1986, 1987) developed a fully relativistic description of hydromagnetic flows in magnetospheres, essentially applicable to any field topology. These results, originally derived for active galactic nuclei, were extended to a self–consistent model of protostellar systems (CA, Camenzind et al. 1994, hereafter CFP), considering the accretion process onto the star as well as the ejection of plasma in magnetized winds or jets.

Heyvaerts & Norman (1989) for the Newtonian case and Chiueh et al. (1991) for relativistic winds showed that magnetized winds will collimate along the symmetry axis. Appl & Camenzind (1993a,b) presented an analytic model of a stationary relativistic magnetized jet in the asymptotic regime. This is the first solution for the relativistic GSS equation with a nonlinear current distribution in the asymptotic domain. The 2D extension of this solution has not been known.

While the protostellar jet phenomenon is relatively common and some people consider it as a regular phase during the stellar evolution, jets from evolved stars like neutron stars or white dwarfs are seldom. Besides the well known famous SS 433 jet originating from a neutron star (D'Odorico et al. 1991) in a binary system and accelerating the mass outflow up to relativistic velocities of about 50000 km s^{-1}, only a few examples are indicated. This is maybe due to a misalignment between the rotational axes of the star–disk system and the stellar magnetosphere.

Our goal is the investigation of the *jet* phenomenon and therefore we will concentrate in this paper mostly on protostellar jets since the obervational basis is quite larger.

We will present different numerical solutions of the 2D force–balance equation which show the collimation process of a dipolar stellar magnetic field to an asymptotic cylindrical jet with finite radius. In our basic assumptions, we follow the model of CFP.

Nevertheless, our results are more general and allow further application to pulsar magnetospheres or other star–disk systems. Similar star–disk scenarios are also applied for relativistic pulsar magnetospheres (e.g. Michel 1991). In particular, the scaling of the stellar radius and the LC for pulsar magnetospheres is of the same order as for protostellar systems (see Table 1).

One may question the special relativistic treatment of the protostellar jet magnetohydrodynamics remembering that the observed jet velocities of about 400 km s^{-1} (Mundt et al. 1987, 1990; Reipurth 1989) are clearly non–relativistic. We argue that the application of relativity could never be wrong since it is the more general theory and it also allows for a smooth transition towards the Newtonian limes. However, one has to make use of the right parameters.

In fact, there a two major aspects to involve relativity (see also Sect. 3). The first one is coming from the model assumption of a global *stellar* magnetosphere and the observed rotational periods of the order of days (Bouvier et al. 1990, 1993). Then, the derived light cylinder (LC, where the rotational velocity of the rigidly rotating stellar magnetic field lines equals the speed of light) is of the order of the observed jet radii of about 10^{15} cm (Mundt et al. 1987, 1990). The rapid rotation (compared e.g. to the sun) generates electric fields which cannot be neglected. The LC, on the other hand, has no direct influence either on the GSS Eq. (8) or on the dynamics of the moving plasma since the "decoupling" of the plasma from the field lines due to inertial forces already happens at the Alfvén surface (see Sect. 2). Because we finally assume a force–free ansatz for the GSS equation, where the Alfvén surface becomes identical to the LC, we were able to use the regularity condition (Sect. 2.4) as a boundary condition at the LC.

The second argument supporting a relativistic treatment is the fact that the plasma loading rate from the disk or the stellar surface into the magnetosphere is not uniform for different flux surfaces. The value for a single flux surface may greatly differ from the observed mass loss rate as a mean across the jet. Low mass loss rates (equivalent to a high plasma magnetization) imply high plasma velocities which may be in the relativistic regime. The numerical investigation of the dynamics of the mass flow is the subject of a forthcoming paper (Fendt & Camenzind 1994).

The structure of the paper is as follows. In Sect. 2 we recall some basic equations of the theory of relativistic magnetospheres and discuss important properties of the GSS equation. In Sect. 3 we present the model on which our numerical calculations are based. In Sect. 4 we introduce the method of finite elements for the GSS equation. Some numerical details are pointed out in Appendix A. We present our numerical results in Sect. 5

and discuss solutions with different topologies and jet parameters. A result concerning not only protostellar jets but generally the theory of global relativistic magnetospheres is discussed in Appendix B.

2. MHD description of magnetospheres

The basic equations describing a magnetohydrodynamic (MHD) configuration under the assumptions of axisymmetry, stationarity and ideal MHD are well known (e.g. Chandrasekhar 1956). Thus, we only briefly review the basic points following the derivation given by Camenzind (1987, 1990). Throughout the paper we use cylindrical coordinates (R, ϕ, Z), respectively (x, ϕ, z) in units of light cylinder radii $R_{\rm L}$.

The magnetospheric structure follows from the force–balance perpendicular to the flux surface. The projection of the equation of motion perpendicular the field lines provides the GSS equation. The projection parallel to the field, i.e. the wind equation, gives the properties of the plasma flow: energy, velocity, density and Mach–number. Both equations have to be solved simultaneously.

Michel's magnetization parameter $\sigma_{\rm M}$ measures the strength of the magnetic flux in terms of the inertial mass flow in the wind (Michel 1973b). For low $\sigma_{\rm M}$ inertial effects may influence the structure of the magnetosphere. Then the GSS equation and the wind equation have to be solved simultaneously to get a self–consistent solution. High magnetic flux reduces the GSS equation to the force–free pulsar equation (Scharleman & Wagoner 1973), where the Alfvén surface coincides with the LC.

MHD conservation laws for the energy E, the angular momentum L, the mass flow per flux tube η and the angular velocity of the field lines $\Omega^{\rm F}$ can be derived from the equation of motion. Therefore, these quantities are only functions of the flux surface Ψ alone. In the force–free limit this holds also for the integral poloidal current $I(\Psi)$.

Since in our model all the field lines are anchored in a small central region around the protostar, we assume a constant angular velocity of the field lines equal to the angular velocity of the protostar

$$\Omega^F(\Psi) = \Omega^F = \text{const.} = \Omega_\star \tag{1}$$

For simplicity, we further assume that gas pressure is negligible in the magnetosphere, i.e. we are dealing with a cold plasma flow.

2.1. The cross–field force–balance

Introducing the magnetic flux function,

$$\Psi = \frac{1}{2\pi}\int \boldsymbol{B}_{\rm P}\cdot d\boldsymbol{A}, \qquad R\boldsymbol{B}_{\rm P} = \nabla\Psi \wedge \boldsymbol{e}_\phi, \tag{2}$$

Ampère's law leads to the Grad–Schlüter–Shafranov equation

$$R\nabla\cdot\left\{\frac{1}{R^2}\nabla\Psi\right\} = -\frac{4\pi}{c}j_\phi. \tag{3}$$

The spatial part of the relativistic equation of motion,

$$(\boldsymbol{u}\cdot\nabla)(\mu\boldsymbol{u}) = \rho_{\rm e}\,\boldsymbol{E} + \frac{1}{c}\,\boldsymbol{j}\wedge\boldsymbol{B} \tag{4}$$

with the spatial part of the 4–velocity $\boldsymbol{u}$, normalized to the speed of light, and the specific enthalpy μ, is then projected perpendicular to the magnetic flux surface. This provides the toroidal current,

$$\frac{1}{c}\,j_\phi\,D = \gamma\,n\,R\,(\partial_\Psi E - \Omega\,\partial_\Psi L) + \frac{R}{4\pi}\left(B_\phi^2 + M^2 B_{\rm P}^2\right)\,\partial_\Psi(\ln\eta) + \frac{R}{R_{\rm L}}\,\rho_{\rm GJ}\,, \tag{5}$$

where $D = 1 - M^2 - x^2$. $\rho_{\rm GJ}$ denotes the Goldreich–Julian charge density,

$$\rho_{\rm GJ} = \frac{\nabla\Psi\cdot\nabla(R^2\Omega^F)}{4\pi R c R_{\rm L}}\,. \tag{6}$$

which is a consequence of the electric field, $E_\perp = (R/R_{\rm L})\,B_{\rm P}$. This is only negligible for $R << R_{\rm L}$.

The relativistic Alfvén–Mach number is given by

$$M^2 = \frac{4\pi\mu\eta^2}{n}\,, \tag{7}$$

with the proper particle density n. D can be absorbed in the divergence term on the l.h.s. and, normalizing with

$$\begin{aligned} R, Z &\Leftrightarrow R_{\rm L}\,x, R_{\rm L}\,z\,,\\ \Psi &\Leftrightarrow \Psi_{\rm max}\,\Psi\,,\\ RB_\phi &\Leftrightarrow (\Psi_{\rm max}/R_{\rm L})\,T\,,\\ E, L &\Leftrightarrow \mu\,E, \mu\,L\,, \end{aligned}$$

one finally ends up with the modified GSS equation

$$x\nabla\cdot\left(\frac{D}{x^2}\,\nabla\Psi\right) = -\frac{1}{\sigma^2}\frac{\gamma x}{M^2}\,(\partial_\Psi E - \Omega\,\partial_\Psi L) - \frac{1}{x}\left(T^2 + M^2|\nabla\Psi|^2\right)\partial_\Psi(\ln\sigma)\,. \tag{8}$$

σ denotes the inverse coupling to the inertial current,

$$\sigma = \frac{\Psi_{\rm max}^2}{2\dot{M}_{\rm jet} c R_{\rm L}^2} = 5\,10^{-7}\dot{M}_{\rm jet,-10}^{-1} R_{\rm L,15}^{-2}\Psi_{\rm max,25}^2\,, \tag{9}$$

and is equal to Michel's magnetization parameter $\sigma_{\rm M}$.

The GSS–equation has some important properties:

(i) The source term on the r.h.s. of the GSS equation is highly nonlinear.

(ii) Within the fast magnetosonic surface the GSS equation is elliptic but changes its character to a hyperbolic type outside.

(iii) Further, we have a free boundary problem since we do not know *a priori* the shape and the location of the jet radius.

(iv) At the Alfvén surface, $D = 0$, the GSS equation has a critical surface which originally is introduced by the toroidal current j_ϕ. The location of the Alfvén surface has to be calculated from the wind equation. The requirement of regularity leads to a condition on the magnetic field component parallel to the surface $D = 0$. This corresponds to an inhomogeneous Neumann condition at boundaries on the Alfvén surface (see below).

2.2. The force–free limit

The force–free limit is characterized by a vanishing inertia, $\sigma \rightarrow \infty$. In this limit, the GSS equation, Eq. (3), reduces to the pulsar equation originally derived by Scharlemann & Wagoner (1973),

$$\frac{1}{c} j_\phi D = \frac{1}{4\pi R} \frac{4}{c^2} I \, \partial_\Psi I + \rho_{\rm GJ} \frac{R}{R_{\rm L}}, \tag{10}$$

with $D = 1 - x^2$. Now the Alfvén radius is identical to the LC, $x_{\rm A} = 1$. The poloidal current $I(\Psi) = (c/2)\, RB_\phi$ flows within the flux surfaces,

$$I(\Psi) = \int \boldsymbol{j}_{\rm P} \cdot d\boldsymbol{A} \,. \tag{11}$$

It becomes a free function and governs now the structure of the magnetosphere. With the normalization

$$I \Leftrightarrow I_{\rm max}\, I, \tag{12}$$

Eq. (3) can be written dimensionless,

$$x \nabla \cdot \{ \frac{D}{x^2} \nabla \Psi \} = - g_{\rm I} \frac{1}{x} I \, \partial_\Psi I \,. \tag{13}$$

$g_{\rm I}$ is the coupling constant for the poloidal current,

$$g_{\rm I} = \frac{4 I_{\rm max}^2 R_{\rm L}^2}{c^2 \Psi_{\rm max}^2} = 4 \, (\frac{I_{\rm max}}{10^{15} {\rm A}})^2 R_{\rm L,12}^2 \Psi_{\rm max,25}^{-2} \,. \tag{14}$$

The coupling constant also measures the contribution of the poloidal currents to the toroidal current density in terms of the Goldreich–Julian current density. This can be seen from Eq. (10) by comparing the (normalized) terms of the r.h.s.,

$$\frac{j_\phi I}{j_{\phi {\rm GJ}}} = g_{\rm I} \frac{I \partial_\Psi I}{\nabla \Psi \cdot \nabla x^2} \,. \tag{15}$$

The normalized quantities T and I are related via

$$T^2 = g_{\rm I} \, I^2 \,. \tag{16}$$

2.3. Plasma motion along the magnetic surfaces

The motion of the plasma along the flux surface is described by the wind equation. In the cold wind limit this equation simplifies to an implicit polynomial in the poloidal velocity $u_{\rm P} = \gamma v_{\rm P}/c$ of degree of 4

$$\sum_{m=0}^{4} A_m(x; E, L, \Phi, \sigma) \, u_{\rm P}^m = 0 \,, \tag{17}$$

(Camenzind 1986, 1987), where the coefficients A_m depend explicitly on the magnetization σ, the flux tube function $\Phi = B_{\rm P} R^2$ and on the constants of motion,

$$E(\Psi) = \gamma - \sigma T \,, \tag{18}$$

$$L(\Psi) = \frac{1}{\Omega^F} \left(x u_\phi - \sigma T \right) \,, \tag{19}$$

with the same normalization as in Eq. (8).

At each radius x, the wind Eq. (17), as a polynomial of degree of 4, may have four different solutions $u_{{\rm P},k}(x)$, $k = 1...4$. We were looking for the branch of a *physical* wind solution $u_{\rm P}(x)$, which starts at zero velocity at the injection radius and passes, monotonically accelerating, the Alfvén point and the fast magnetosonic point. This solution determines the energy of the plasma flow.

2.4. The role of the Alfvén surface

Evaluating Eqs. (8) or (13) at the Alfvén surface, $x = x_{\rm A}$ gives

$$\frac{\partial \Psi}{\partial n} = - \frac{x_{\rm A}}{|\nabla D|} \, J \,, \quad \boldsymbol{n} = - \frac{\nabla D}{|\nabla D|} \,, \tag{20}$$

where J denotes the r.h.s. of Eqs. (8) or (13) and $\boldsymbol{n}$ the unit vector normal to the Alfvén surface.

This regularity condition has to be satisfied by all field lines passing this surface. Thus, Eq. (20) provides a boundary condition for integration domains with boundaries on the Alfvén surface. Therefore, it is possible to solve the GSS independently on domains within and outside $x_{\rm A}$, as already mentioned by other authors (Scharlemann & Wagoner 1973; e.g. Michel 1991).

It is important to note that the regularity condition also gives a condition on the shape of the jet boundary at $x_{\rm A}$. Since the jet boundary has to follow the outermost flux surface (by definition), its slope is restricted by the regularity of this surface $\Psi = 1$. However, the slope of the field lines is not fully determined, because the regularity requirement yields only a condition on the magnetic field component parallel to the Alfvén surface, while the slope of the poloidal field is defined by both components of $\boldsymbol{B}_{\rm P}$.

3. The star–disk–jet system

Our astrophysical model for protostellar magnetospheres consists of three main components (see Fig. 1 and CA, CFP):

3.1. The stellar object

The central protostellar object carries a dipolar magnetosphere of about 1000 G. This field strength can be derived from observations of X–ray flares (Montmerle et al. 1993), optical periodicity (Bouvier et al. 1990, 1993) and radio data (André et al. 1988, 1991) as well as from theoretical arguments treating the accretion process (CA, Königl 1991) or a fully convective protostellar dynamo process (CFP). Stellar rotational velocities are typical of the order of 20 km s^{-1} at a stellar radius $R_* \simeq 3 R_\odot$ (Bouvier 1990), the derived rotational periods are in agreement with other results of direct detections of the order of days (Bouvier et al. 1993). Then, the LC is located at $R_{\rm L} \simeq 10^{15}$ cm or $R_{\rm L} \simeq 5000 R_*$.

Like fast rotating pulsar magnetospheres the protostellar magnetosphere cannot be in vacuum: Due to the fast rotation the electric field parallel to the flux surface $\boldsymbol{E}_\parallel$ exceeds the gravitational force by a large factor and will therefore create a space

charge ρ_{GJ} until the magnetic field lines become equipotentials again (Michel 1991). For a typical TTS this factor can be estimated to 10^{10} (for protons), demonstrating the necessity of a relativistic treatment of protostellar magnetospheres. Numerical calculations of Neukirch (1993) show that plasma will populate the magnetosphere until the charge density approaches ρ_{GJ} in the plasma filled region where $E_{\parallel}$ is then screened out.

Nevertheless, the density of a stellar wind of typical mass loss rates observed for TTS is much larger than the Goldreich–Julian charge density. This allows for a magnetohydrodynamic description of the problem.

One may wonder about how a *stellar* magnetic field is able to continuously influence the plasma flow far out to thousands of stellar radii. This would question our very basic model assumption of the global jet magnetosphere as a collimated stellar magnetic field. Besides the fact that most of the disk wind models considered in the literature also assume the closest circumstellar environment as the jet origin as well (e.g. Pelletier & Pudritz 1992), we refer to the solar magnetic field which is known to extend to the distance of about 70 AU, a value near the observed protostellar jet radii.

Observations show that the gas outflow consists of hot and ionized components even at distances of several hundreds of AU from the stellar object. Temperatures of about 10^4 K and typical electron densities of about $10^4\,\mathrm{cm}^{-3}$ are derived in the stellar wind (e.g. Edwards et al. 1987) as well as in the asymptotic jet (e.g. Mundt et al. 1990). The ionized gas couples to the magnetic field. However, the cooling of the expanding flow is strong (Hartmann & Raymond 1989) and the physical mechanism reheating the gas far from the star is not yet clearly known. Safier (1993) suggested ambipolar diffusion as a robust mechanism heating the gas and calculated ionization fractions of $\sim 0.1 - 1$ at distances of $\sim 100 - 1000$ AU from the star. Although his result is based on a model assumption different to ours (i.e. a self–similar disk wind) it strengthens our MHD assumption of a ionized plasma flow coupled to a far reaching magnetosphere. For our results this assumption has to be finally reconfirmed by the calculation of the parameters of the plasma dynamics and the energy dissipation of the plasma flow.

3.2. The accretion disk

The interaction of the accretion disk with the stellar magnetic field produces a gap (Gosh & Lamb 1978, CA). The inner radius of the disk R_{in} is determined by pressure equilibrium between the stellar magnetic field and the accretion flow of the disk. An accretion rate $\dot{M}_{acc}$ of the order of $10^{-7} M_{\odot}\mathrm{yr}^{-1}$ (Beckwith et al. 1990) provides $R_{in} \simeq 3R_*$ for stellar fields $B_\star \simeq$ kG.

The maximum poloidal current driven through the disk can be estimated to $I_{max} \simeq 10^{15}$ A (CA). Whether such a strong current will flow up into the asymptotic jet or will be concentrated mainly into the innermost part of the magnetosphere is not known a priori. Observations indicate that the net jet current may be smaller by a factor of $\simeq 1000$ (see below).

For a disk with high resistivity, the protostellar magnetic field will penetrate the disk. This will lead to a *reversed field pinch* in asymptotic regime *(model ARP)*. A concentration of field lines at the innermost part of the disk is required to satisfy our assumption of a constant angular velocity of field lines.

For a disk with low resistivity, the stellar dipole is closed only in the gap between star and disk. All field lines reaching the asymptotic regime originate from the stellar surface leading to an *asymptotic monotonous* flux distribution (*model AMP*).

The injection mechanism for jet plasma is quite different in the two scenarios:

(1) In a field topology of model ARP, we are dealing with a classical disk wind: Plasma will be flung out along field lines emanating from the disk beyond the corotational radius. In this scenario, the plasma flow is mainly concentrated in the outer flux surfaces of the jet. In the asymptotic region, the jet will be hollow.

(2) In a topology of model AMP, the mass injection happens similar to a stellar wind. Plasma will flow in all flux surfaces reaching from the stellar surface to the asymptotic regime. In addition, disk material may enter the wind regime by Rayleigh–Taylor or Kelvin–Helmholtz instabilities.

In comparison, the first mechanism provides a higher mass flow, while the other will accelerate more efficiently due to the fast rotation of the foot points of the flux tubes.

Both topological configurations allow for mass infall along the dipolar loops which close onto the stellar surface. Numerical calculations treating this accretion scenario are presented by Paatz & Camenzind (1994).

3.3. The asymptotic jet

Heyvaerts & Norman (1989) have shown that jets carrying a poloidal current collimate asymptotically to a cylindrical geometry. Indeed, highly collimated outflows with velocities of the order of $400\,\mathrm{km\,s}^{-1}$ are observed.

The observed protostellar jet radii are of the order of 10^{15} cm (Mundt et al. 1987, 1990) and are therefore of the order of the LC. As already declared, this observational constraint motivates a relativistic treatment despite the small velocities of the Newtonian stellar system.

The asymptotic jet further is determined by the distribution of the integral poloidal current as well as the strength of the current. In our calculations we use a nonlinear distribution derived in the asymptotic jet equilibrium (Appl & Camenzind 1993b). From energy equilibrium arguments in the jet, Mundt et al. (1990) derived a toroidal magnetic field of 60 μG, which implies a poloidal current $I_{max} \simeq 10^{12}$ A. As mentioned above, this value is smaller by a factor of 1000 than currents derived in the accretion disk. It should be noted that there exist examples where, similarly, the mass flow in the jet, derived from observations to $\dot{M}_{jet} \simeq 10^{-10} M_{\odot}\mathrm{yr}^{-1}$ (Mundt et al. 1987) and the accretion rate in the disk differ by nearly the same factor. In general, the mass loss rates into the jets are discussed to may be higher more than two orders of magnitude (e.g. Königl & Ruden 1993). Then, the plasma magnetization would change by the same order of magnitude. But this does not influence the results presented in this paper because of the force–free assump-

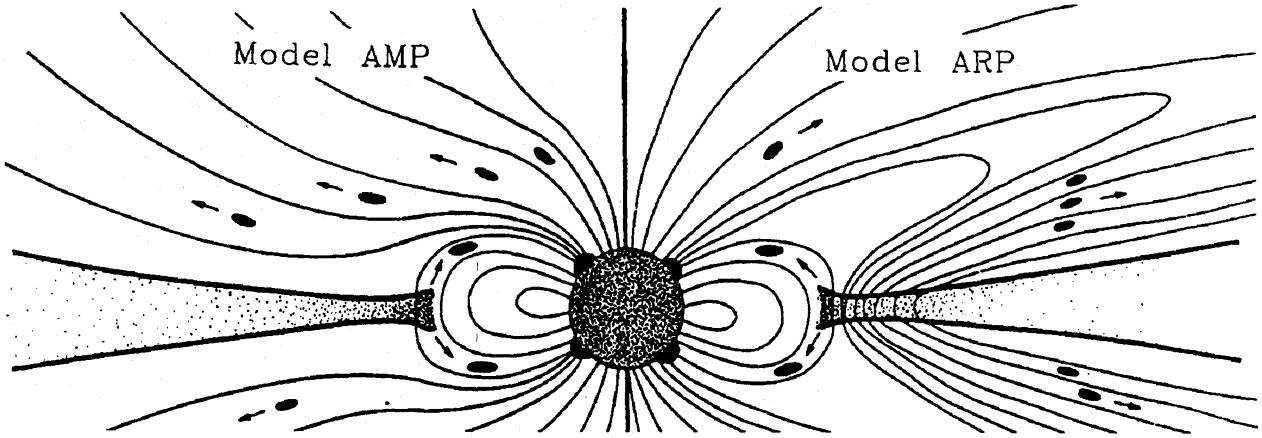

Fig. 1. Model of the innermost region of a protostellar jet source. The central protostellar object, a classical TTS or an embedded IR source, is surrounded by a stellar dipolar magnetic field and an accretion disk. The asymptotical topology of the field (here indicated as poloidal field lines or axisymmetric flux surfaces) is determined by the assumption of the resistivity in the disk (see text). The sketch shows on the l.h.s. the AMP topology and on the r.h.s. the ARP topology, respectively. Arrows indicate the direction of the mass flow (filled bubbles). Mass infall along the dipolar field lines leads to an accretion ring on the stellar surface at high latitudes. Picture taken from Fendt (1994)

Table 1. Comparison of characteristic parameters of stellar magnetospheres and jets. Rotational periods P and stellar radii $R_\star$ of TTS taken from Bouvier et al. (1993), jet radii $R_{\rm jet}$ from Mundt et al. (1987, 1990)

	$R_\star$ in $R_\odot$	P	Ω^F in s^{-1}	$R_{\rm L}$ in cm	in AU	in $R_\star$	$R_{\rm jet}$ in cm	in $R_\star$	in $R_{\rm L}$
TTS	$\lesssim 3$	$1\overset{d}{.}0$	$7.3\,10^{-5}$	$4.1\,10^{14}$	28	~ 2000	$\sim 1-10\,10^{15}$	$\sim 5-50\,10^3$	$\sim 2-10$
		$5\overset{d}{.}0$	$1.5\,10^{-5}$	$2.1\,10^{15}$	138	~ 15000			
DG Tau	2.1	$6\overset{d}{.}3$	$1.15\,10^{-5}$	$2.6\,10^{15}$	174	17800	$4.2\,10^{15}$	29000	1.6
Pulsars	$\sim 10^{-5}$	$1\overset{s}{.}0$	2π	$4.8\,10^9$	$3.2\,10^{-4}$	~ 4800			
Sun	1.0	$25\overset{d}{.}4$	$2.9\,10^{-6}$	$1.1\,10^{16}$	700	$1.5\,10^5$			

tion for the magnetosphere. It will, however, strongly affect the properties of the wind flow in the magnetosphere and will be considered in a forthcoming paper where we investigate the dynamics of the plasma as a function of the mass loss rate (Fendt & Camenzind 1994).

3.4. Boundary conditions

The computations have to satisfy the following boundary conditions.

(1) Along the protostellar surface the flux function is given by a dipolar magnetic field (Dirichlet boundary).

(2) $\Psi(0, z) = 0$ on the rotational axis.

(3) The gap between the stellar surface and the inner edge of the disk is represented by a homogeneous Neumann boundary condition $\partial_n \Psi = 0$.

(4) Ψ satisfies a Dirichlet condition along the disk surface. In model ARP the stellar magnetic field will enter the disk with

$$\Psi_{\rm disk}\,(x, h(x)) = \Psi_{\rm star}\left(\frac{x_{\rm in}}{x}\right)^m, m \geq 4\,, \qquad (21)$$

while in model AMP

$$\Psi_{\rm disk}\,(x, h(x)) = \text{const.} = \Psi_{\rm star}(x_{\rm in}, 0). \qquad (22)$$

Given by the high power in Eq. (21), the foot points of the flux surfaces are concentrated to the innermost region. This allows for the assumption of a rigid rotation of the magnetosphere. For radii of the order of several $x_{\rm in}$ the curve $(x, h(x))$ denotes the surface of the disk, while for $x \gg x_{\rm in}$ it just describes the jet boundary and we fix $\Psi(x, h(x))$ similar as in the disk region. The function $h(x)$ has to be well adjusted to the regularity requirement (s. Appendix B).

(5) At the upper boundary $(x, z_{\rm out})$ we assume that the jet has been collimated into a cylindrical shape. Thus, we use either homogeneous Neumann conditions or the analytic solution of the asymptotic jet equilibrium as a Dirichlet condition. When the outer and inner domain are calculated separately, then Dirichlet conditions are required at the upper boundary. Otherwise it would not be possible to fix the flux in this domain.

(6) For integration domains with boundaries on the Alfvén surface *no* boundary condition has to be given there. In our finite element approach the regularity condition is *automatically*

satisfied. Like the homogeneous Neumann condition the regularity condition is a natural boundary condition on $D = 0$ in the sense that the surface integral (s. Eq. (29)) does not contribute. The accuracy of this surprising result is assured by different numerical tests.

3.5. The current distribution

For the integral poloidal current in model AMP we use the asymptotic analytical solution for relativistic pinches given by Appl & Camenzind (1993b),

$$I(\Psi) = \frac{1 - e^{-b\Psi}}{1 - e^{-b}} \,. \tag{23}$$

The strength of the current, g_I, and the shape of the profile ($b \ll 1$ diffuse pinch, $b \gg 1$ sharp pinch) control the magnetic structure and the kinematics of the jet. They determine in particular the asymptotic jet radius and velocities. Here we choose g_I and b such that it yield a jet radius of a few LC radii.

The jet possesses a core–envelope structure (Appl & Camenzind 1993b). In the asymptotic profiles of $\Psi(x), I(x)$ the so called core radius a plays the role of a typical length scale. For $x << a$ magnetic flux and poloidal current increase with radius. For $x >> a$ the poloidal current approach a constant value, corresponding to a vanishing current density. Thus, the current flow is concentrated within the core radius. As shown by Appl & Camenzind (1993b), the same holds for the Poynting flux. High $g_\mathrm{I} \simeq 10^4$ will lead to core radii a of several stellar radii. In this case the jet is a sharp pinch, while for a weaker coupling the core radius becomes of the order of the jet radius and a diffuse pinch results.

In the case of model ARP $I(\Psi)$ is required to have a maximum, since the topological transition between the dipolar type magnetosphere to a cylindrical jet provides a singular sheet and a critical flux surface Ψ_cr with $j_\mathrm{P}(\Psi_\mathrm{cr}) = 0$. We therefore use

$$I(\Psi) = \mathrm{e}^2 \left(\frac{\Psi}{\Psi_\mathrm{cr}} \right)^2 \mathrm{e}^{-2\Psi/\Psi_\mathrm{cr}} \,. \tag{24}$$

4. Numerical techniques

4.1. Finite element solver

The GSS equation is solved by means of the method of finite elements (Camenzind 1987). For this purpose we multiply Eq. (13) by a test function N (Galerkin ansatz) and integrate over the 2D plasma domain G applying Green's identity. We end up with the *weak form* of the GSS equation,

$$\int_G \frac{D}{R} \nabla N \cdot \nabla \Psi \, dR \, dZ = \int_G J \, N \, dR \, dZ + \int_{\partial G} \frac{D}{R} \, N \frac{\partial \Psi}{\partial n} \, dS, \tag{25}$$

where n now denotes the unit vector perpendicular to the boundary ∂G.

The plasma domain G is discretized in a set of isoparametric curvilinear 8–node elements of the serendipity class (Schwarz 1984). The discretization has to be fine enough to resolve the star–gap–disk system. With a 64 x 64 element grid, we were able to scale R_L to 100 R_* and $R_\mathrm{jet} \leq 1000\, R_*$. In Fig. 8 (Appendix A) we show an example of a grid used in our computations.

Within each element the flux function Ψ is expanded as

$$\Psi(R, Z) = \sum_{i=1}^{8} \Psi_i^{(e)} \, N_i(\zeta, \eta). \tag{26}$$

$\Psi_i^{(e)}$ denote the magnetic flux at the nodal point i of the element (e) and (ζ, η) are rectilinear coordinates on the normalized element. The shape function N_i is unity at each node i and varies quadratically with ζ or η on the edge of the element. Other physical quantities as R, Z, j_ϕ can be expanded in the same way. Since the l.h.s. of Eq. (13) changes sign on the Alfvén surface x_A, one coordinate line of the numerical grid has to follow the surface $D = 0$ in order to allow a coordinate transformation from the physical curvilinear element grid (x, z) to the normalized element the (ζ, η).

Following the Galerkin scheme we select the shape functions N_i as test function and finally obtain a system of nonlinear equations for Ψ at all nodal points,

$$\mathsf{A}(\Psi) \, \Psi = \boldsymbol{b}(\Psi), \tag{27}$$

with the integrals on each grid element

$$A_{ij}^{(e)} = \int_{G_e} \frac{D}{x} \left(\partial_x N_i \, \partial_x N_j + \partial_z N_i \, \partial_z N_j \right) dx \, dz, \tag{28}$$

and

$$b_i^{(e)} = \int_{G_e} N_i \, J^{(e)} \, dx \, dz \; + \int_{\partial D} \frac{D}{x} \, N_i \, \partial_n \Psi \, ds. \tag{29}$$

Each component of Eq. (27) corresponds to the force equilibrium between neighbouring nodal points of each element. Inversion of matrix Eq. (27) yields the solution Ψ on the nodal points. The expansion (26) provides the solution in any point $\Psi(x, z)$.

The gradient of Ψ follows from the derivation of Eq. (26)

$$\nabla \Psi^{(e)} = \sum_{i=1}^{8} \Psi_i^{(e)} \, \nabla N_i(\zeta, \eta) \,. \tag{30}$$

Since we are using *quadratic* elements, the gradients will not be necessarily continuous at the element boundary. This is important for solving the wind equation, where the flux tube function $\Phi = x \, |\nabla \Psi|$ is used. For that purpose one has to smooth the flux tube function such that the gradient becomes continuous.

The finite element solver allows for a calculation on the entire jet domain as well as for a separate computation inside and outside the Alfvén surface, respectively. The calculation on the entire domain requires only an inner Dirichlet boundary condition on Ψ, while in the case of a separate calculation we need an additional Dirichlet condition for the outside domain.

4.2. Numerical tests

We found several possibilities to test the accuracy of our numerical technique in the force–free limit.

At first, appropriate boundary conditions provide a solution to the classical pulsar equation (s. Fig. 9a, Appendix A). Comparison with the exact result from Michel (1973b), derived with a totally different method shows practically no deviation in the field line configuration. The value of the critical flux surface as well as the cusp angle coincide perfectly. Note that we have *not* used a boundary condition at the LC: The homogeneous Neumann condition as a natural boundary condition is automatically satisfied.

In a second test, we transformed the exact monopole solution derived by Michel (1973a) to a monopole type distribution more comparable to the model topology AMP,

$$\Psi(x,z) = 1 - \frac{z}{(x^2+z^2)^{1/2}}, \qquad I(\Psi) = 1 - \Psi^2, \tag{31}$$

and, using this analytical result as boundary condition, we found exactly the same distribution over the whole regime (s. Fig. 9b, Appendix A). The solver is absolutely stable in the regime around the LC where the calculated distribution of Ψ as well as $\nabla\Psi$ is continuous and show no kinks. In this example, the calculation was performed on the entire integration domain. A composition of separate solutions for the regime within and outside the LC gives the same result. Again, the regularity condition was automatically satisfied without any boundary condition at the LC.

In a third test, we compared the numerical calculation with the analytic 1D asymptotic solution of Appl & Camenzind (1993b). We solved the GSS equation in a rectangular domain along the asymtotic jet using homogeneuous Neumann conditions at the upper and lower boundary. Then, the 2D solution coincides with the 1D analytical distribution. This behavior can also be seen in the asymptotic regime of the astrophysical solutions, where the solver perfectly finds the analytic result even when Neumann boundary conditions instead of Dirichlet are prescribed.

5. Results and discussion

We now present solutions for the wind and the magnetosphere. In a first approximation the magnetosphere, i.e. the GSS equation has been traced in the force–free limit. As an initial application, the wind equation is solved along a certain force–free flux surface. That inertial forces do not strongly influence the structure of the magnetosphere could be derived from results of Sakurai (1985, 1987) which show only a weak collimation of a monopolar magnetic field by inertial forces. The force–free limit holds for a small plasma loading. Though our calculations are not entirely self–consistent, these are the first calculations of a collimated jet of finite radius from a dipolar stellar magnetosphere.

As already mentioned in Sect. 2.2, the Alfvén surface of the force–free magnetosphere is identical with the LC. The Alfvén surface of the plasma flow depends on the magnetization of the plasma as well as on the structure of the underlaying magnetosphere and would be located somewhere within the LC. In order to calculate this surface from the solution of the wind equation, a reasonable first guess about the structure of the magnetosphere is needed. The only way to treat the problem, is to combine the results of the mGSS equation and the wind equation in an iterative way until our final goal, a self–consistent solution of the non force–free mGSS equation, is obtained. The collimated force–free jet magnetosphere presented in this paper provides an excellent initial solution for the iteration process mentioned above. In a forthcoming paper (Fendt & Camenzind 1994) we will investigate the dynamics of the plasma flow in the collimated magnetosphere presented here. This will include the calculaton of the critical surfaces as well as the derivation of some kinematic properties of the asymptotic jet.

A fundamental problem for the calculation of relativistic force–free magnetospheres is introduced by the singularity of the GSS equation. As known from the treatment of pulsar magnetospheres, global solutions which extend beyond the LC, are found to show kinks at the LC (Ingraham 1973; Pelizzari 1974; Sulkanen & Lovelace 1990; Michel 1991). Obviously, it is not possible to solve the wind equation along such a kinky flux surface. Thus, it became a major prospect of this work to find global solutions of the GSS equation which are well behaved at the LC.

Indeed, in the case of model topology AMP, we found solutions without kinks at the LC. The procedure and a possible physical explanation of this finding is described in Appendix B. It is important to note that in our solutions the regularity at the LC determines the shape and the location of the jet radius $R_{\rm jet}(Z)$.

5.1. The central domain

Figure 2 shows subsets of the innermost part around the stellar object of solutions for both model topologies. As introduced in Sect. 3.2, the disk bondary condition determines the topology of the entire magnetosphere.

Despite the different injection mechanisms for the wind plasma, the flux tubes bridging the inner edge of the accretion disk with the stellar surface, are quite similar. We therefore expect no significant difference in the accretion process. However, mass inflow in model ARP seems to reach a higher stellar latidude implying a smaller extent of the polar accretion "ring".

One may expect that the force–free assumption may break down at first in this regime due to the high accretion mass flow $\dot{M}_{\rm acc} \simeq 100\dot{M}_{\rm jet}$ and that a self–consistent calculation of the accretion may deform the dipolar structure quite strongly. However, for the accretion flow along a dipolar magnetosphere of pulsars (Lamb 1989) or protostars (Paatz & Camenzind 1994) it is known, that it remains sub–Alfvénic. Thus, the accretion process would stay magnetically dominated and the configuration in the innermost part of our solution would be reasonable.

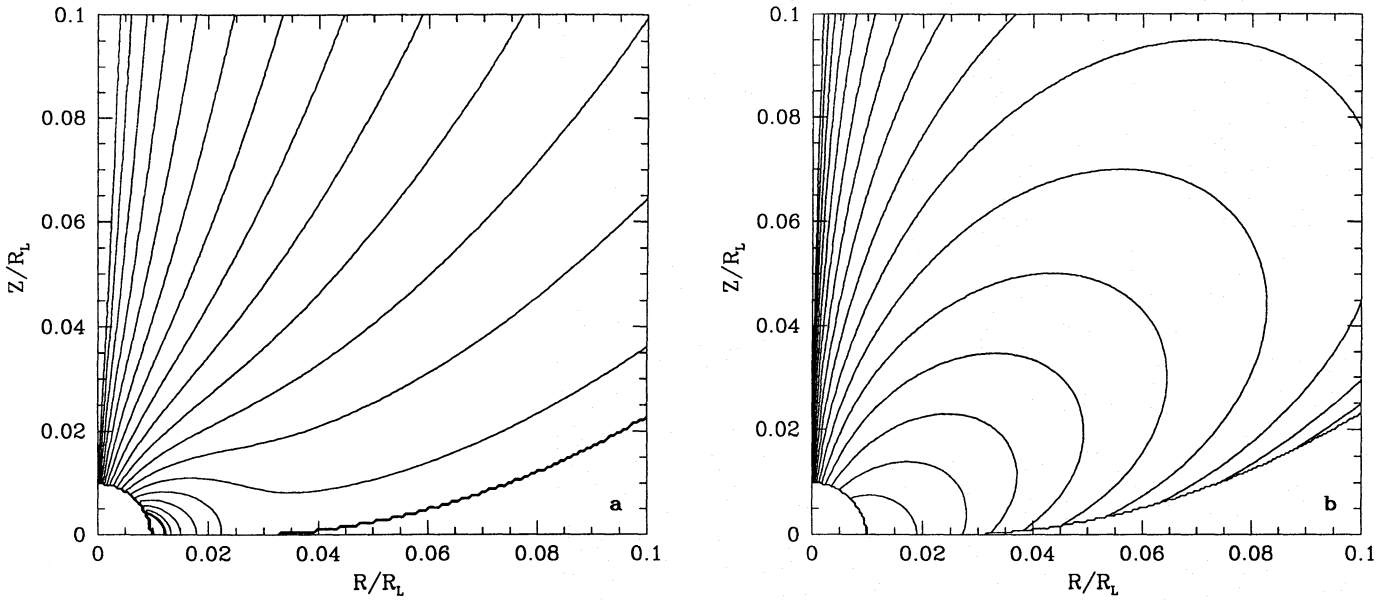

Fig. 2a and b. Magnetic flux surfaces in the innermost part around the protostar. **a** Model AMP, **b** model ARP. Both plots are subsets of the innermost part of the global solutions shown in Figs. 3a and 7. Contour levels: **a** $2\ 10^{-n^2}, n = 0, 1.8, 0.1$; **b** $10^{-n}, n = 0, 5, 0.3$

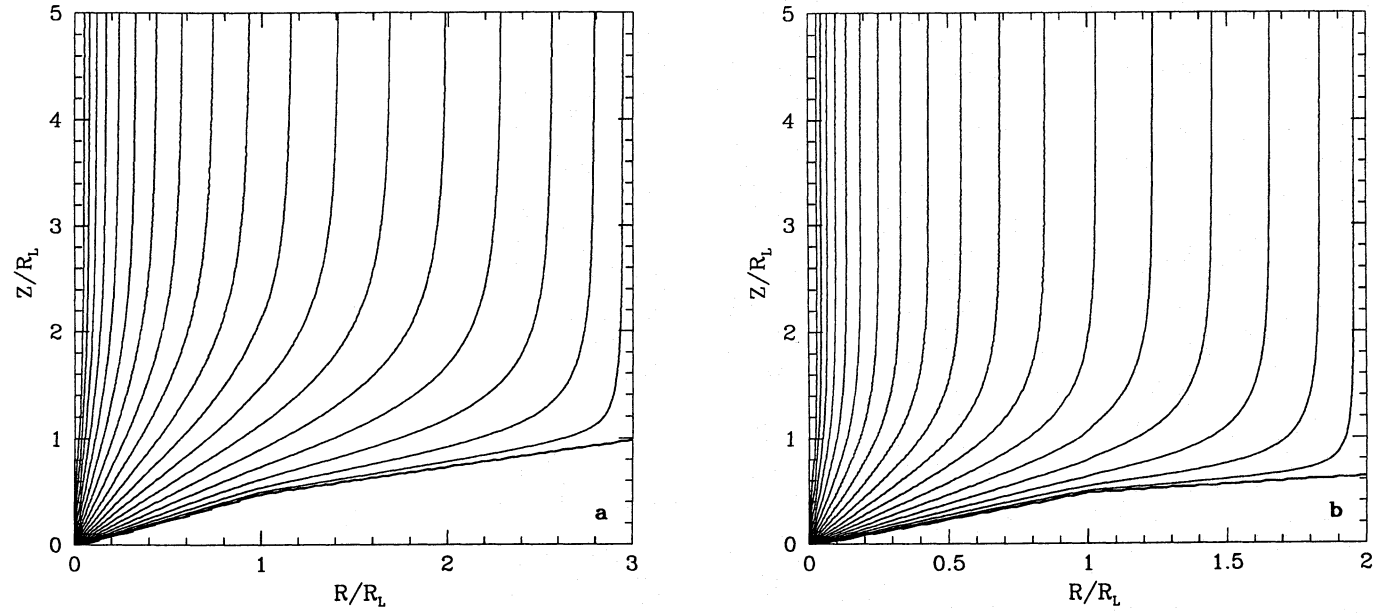

Fig. 3a and b. Magnetic flux distribution $\Psi(x, z)$ for model toplogy AMP with different jet radii. The jet boundaries are adjusted until the kinks at the LC disappear. Parameters: **a** $b = 1.0$, core radius $a = 2.29$, $x_{\rm jet} = 3.0$, $g_{\rm I} = 1.9$; **b** $b = 1.5$, $a = 1.07$, $x_{\rm jet} = 2.0$, $g_{\rm I} = 2.0$. Contour levels: $10^{-n^2}, n = 0, 1.8, 0.1$

5.2. Model topology AMP

The results for the model topology AMP benefit from the knowledge of the solution in the asymptotic regime because we were able to fix the jet radius for large z. Further, with the use of the asymptotic flux distribution it is possible to solve the GSS equation outside the LC independently and investigate the matching problem (s. Appendix B).

The fundamental parameters of solutions of this model topology are given with

- the asymptotic jet radius $x_{\rm jet}$
- and the parameter b of the current distribution.

These parameters determine the coupling $g_{\rm I}$, respectively the strength of the poloidal current. While the asymptotic solution is principally defined for a wide range of $b, x_{\rm jet}, g_{\rm I}$, we find only solutions to a quite limited set of parameters. This may result

from restricted numerical resolution and the choice of the starting configuration for the iteration process. For asymptotic jet radii of several LC we are restricted to $1 \leq b \leq 5$. Then $g_{\rm I}$ is of order of unity. To get solutions with higher coupling one has to use the low b solution as starting configuration and therefore, a further iteration process in the parameter b is necessary. This is in general very time consuming due to the exponential character of the current distribution. Additionally, it does not exactly conserve the analytic equilibrium solution $\Psi(x)$, although the iteration process in each b–step converges.

Figure 3 shows solutions with asymptotic radii $x_{\rm jet} = 3.0, 2.0$ and $b = 1.0, 1.5$. The 2D structure of both solutions is quite similar. The conical distribution of the flux surfaces asymptotically changes to a cylindrical geometry. The collimation process happens fast within a distance of $\simeq 0.3\, x_{\rm jet}$ along the jet axis. This is consistent with observations showing that many protostellar jets optically appear already collimated.

The results of Sakurai (1985, 1987) show that even for solutions which take into account the plasma inertia, a *fast* self–collimated magnetic field structure could hardly be obtained. We therefore conclude that the plasma inertia does not strongly influence the structure of the magnetosphere and the solutions presented in this paper do well describe the magnetic field in a protostellar jet. We believe that fast collimated jet solutions only could be obtained with a fixed outer jet boundary.

The fixed outer jet boundary may interpreted as given by a pressure equilibrium between the jet and the surrounding interstellar medium. In this sense the fast collimation is due to the pressure of the molecular cloud. Therefore, protostellar jets seem not to be self–collimated, but pressure–collimated. The cylindrical shape would correspond to a constant pressure in the molecular cloud. However, for a discussion of the collimation process itself one has to consider the gas pressure of the jet and the surrounding medium as well as the interacting forces between them. We address this question to a future paper. The asymptotic collimation of a force–free jet is subject of the work of Appl & Camenzind (1993a,b).

The initial opening angle in the presented solutions is 65°. Since the slope of the inner jet boundary is not a free function but follows from the regularity condition respectively from the poloidal current distribution, we interpret the inner part of the above solutions as a free expanding wind or jet, whose boundary is solely determined from the force equilibrium inside the jet.

The coupling constant in both solutions is quite similar and corresponds to a maximum poloidal current of $I_{\rm max} \simeq 3.5\, 10^{10}$ A. The strength of the toroidal magnetic field at the jet boundary in the asymptotic region is $B_\phi = 4.6\,\mu$G while that of the poloidal field is $B_{\rm p} = 1.4\,\mu$G. This is in agreement with estimates of the pre–bow–shock magnetic field strengths following observations of HH 111 or HH 34 (Morse et al. 1992, 1993). Zeeman OH measurements for the interstellar magnetic field in the HL Tau region give similar results (Kazes & Crutcher 1986).

Figure 4 shows the 2D distribution of the source term of the GSS equation, $J = (g_{\rm I}/x) I\, I'$, of the poloidal and toroidal field strengths, the pitch angle $\alpha = \arctan(B_{\rm p}/B_\phi)$ and the magnetic pressure $p = (1/8\pi)(B_{\rm p}^2(1-x^2)+B_\phi^2)$ for the solution presented in Fig. 3a. Interestingly, the source term $J(x, z)$ shows a distribution topologically different from the magnetic flux function $\Psi(x, z)$. This is due to the nonlinear current distribution $I(\Psi)$ which provides a maximum in the toroidal current density $j_\phi(\Psi)$ as well as a maximum in the toroidal field strength. As pointed out above, this corresponds to a core–envelope structure in the asymptotic regime.

Figure 5 shows magnetic field configurations with a topological structure different from the solution in Fig. 3a. In the solution shown in Fig. 5a the kinks at the LC could be removed by a variation of the jet boundary in radial extent leading to a kind of recollimation of the flux surfaces. This solution converges to the same asymptotic jet equilibrium as shown in Fig. 3a, since the asymptotic jet radius and the parameter b for the current distribution are the same.

The solution in Fig. 5b is calculated for a concentrated distribution of the poloidal current, $b = 4.5$, resulting in a concentration of the magnetic flux in the inner part of the asymptotic jet. This kind of solutions could only be obtained by iteration from small b and the kinks at the LC could not be fully removed. The concentration of magnetic flux is described by the core radius a of the flux distribution (s. Sect. 3.5). The current flow as well as the Poynting flux are concentrated within the jet core (Appl & Camenzind 1993b). While the solutions in Fig. 3 only show a weak core–envelope structure with core radii of 76%, respectectively 53% of the jet radii, the magnetic flux in the solution in Fig. 5b is concentrated within 11% of the jet radius. Note that we have used the same contour levels in the Figs. 3 and 5. Since the current distribution corresponds to the mass flow in the jet, a concentrated current distribution will correspond to a concentrated mass flow or high densities, respectively high velocities in the inner part of the jet. Thus, this topology is of particular interest for the interpretation of the observed emission line structure with small radial extension in the jet of DG Tau (Kepner et al. 1993; Solf & Böhm 1993).

5.3. *Application: cold wind flow*

In this section we give examples for the solution of the wind equation along a particular flux surface our model AMP configuration (s. Fig. 3a). We demonstrate the dependency of the velocity on the plasma magnetization and point out some interesting aspects of the steady plasma motion. However, we emphasize that the derived absolute values of the plasma velocity could hardly be applied for protostellar jets. In general, they are too high, a fact which is introduced by the strong magnetization of the plasma in our solutions. As shown in Eq. (9), the magnetization of protostellar jets is of the order of $\sigma \simeq 10^{-7}$. Due to numerical reasons, in particular because of the scaling of the stellar radius and the LC, we were not able to calculate a wind with such a low magnetization yet. A more detailed discussion of protostellar jet velocities including a 2D treatment of the plasma dynamics will be the subject of a subsequent paper (Fendt & Camenzind 1994). We note that the asymptotic velocity distribution across the jet could only be derived from a

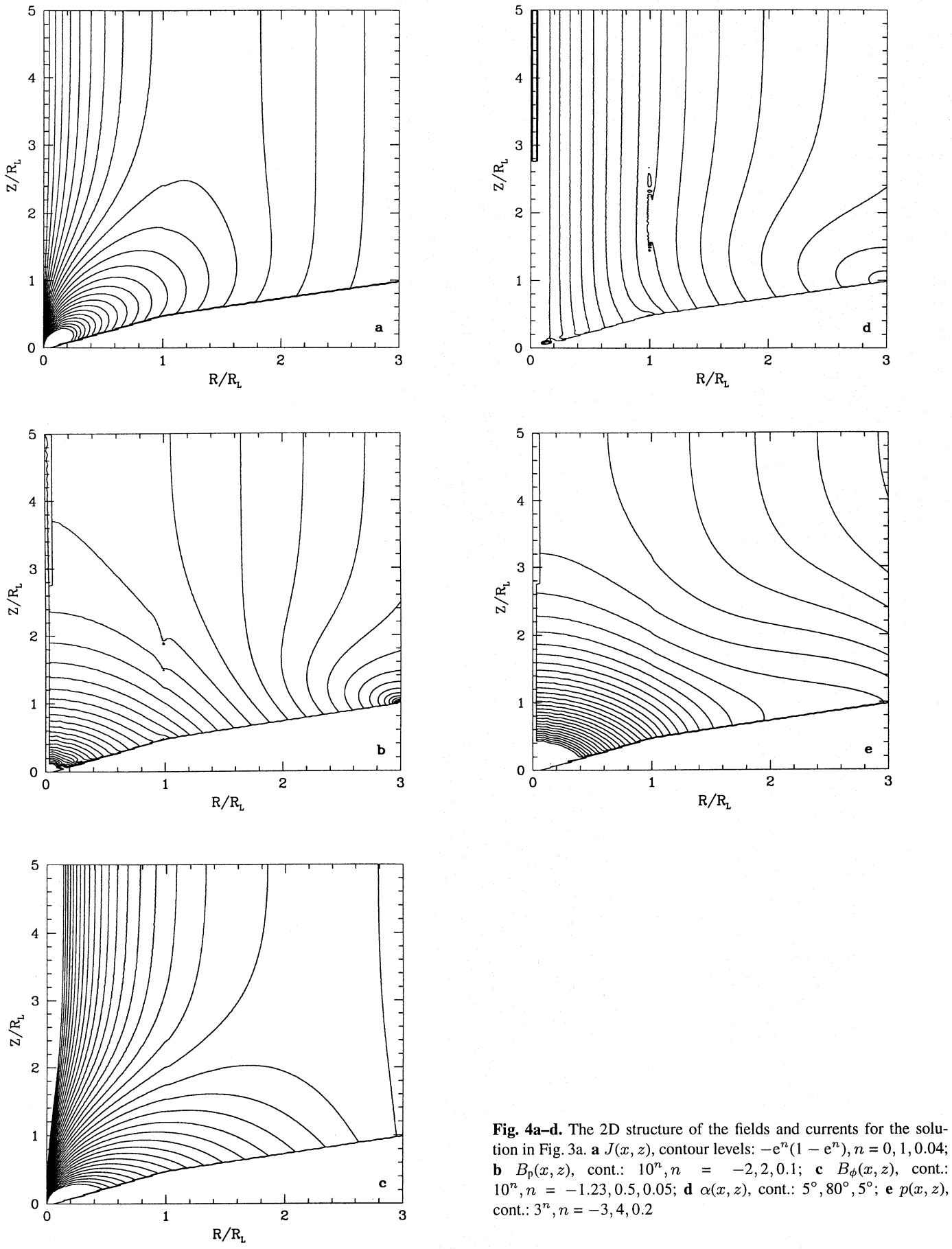

Fig. 4a–d. The 2D structure of the fields and currents for the solution in Fig. 3a. **a** $J(x,z)$, contour levels: $-\mathrm{e}^n(1-\mathrm{e}^n), n = 0, 1, 0.04$; **b** $B_\mathrm{p}(x,z)$, cont.: $10^n, n = -2, 2, 0.1$; **c** $B_\phi(x,z)$, cont.: $10^n, n = -1.23, 0.5, 0.05$; **d** $\alpha(x,z)$, cont.: $5°, 80°, 5°$; **e** $p(x,z)$, cont.: $3^n, n = -3, 4, 0.2$

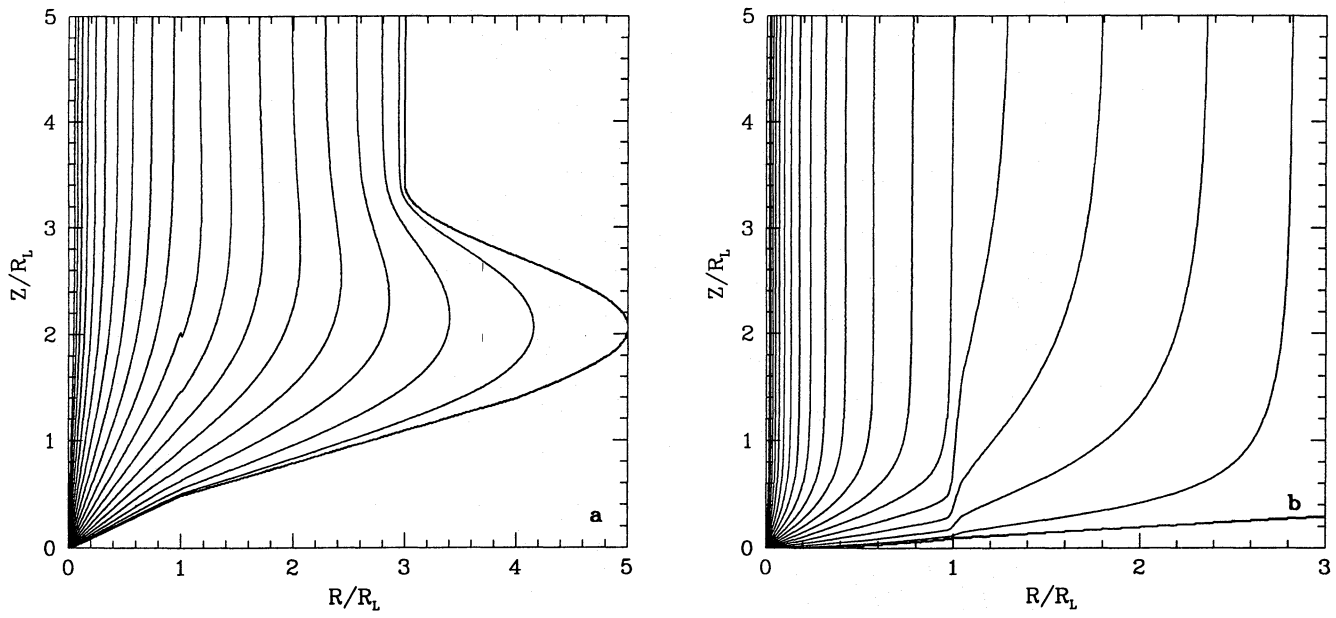

Fig. 5a and b. Magnetic flux configuration $\Psi(x, z)$ with a recollimation structure (a) and a highly pronounced core–envelope structure (b). Parameters: **a** $b = 1.0$, $a = 2.29$, $x_{\rm jet} = 3.0$, $g_{\rm I} = 1.9$; **b** $b = 4.50$, $a = 0.32$, $x_{\rm jet} = 3.0$, $g_{\rm I} = 2.2$. Contour levels as in Fig. 3

2D treatment, since the finite jet radius prevents an asymptotic consideration $R \rightarrow \infty$. Additionally, it would hardly be possible to find the adequate *critical* wind solution in the 1D limit. This solution, which passes the critical magnetosonic surface smoothly, is extremly sensitive on the total energy of the flow $E(\Psi)$.

Figure 6a shows the wind solution in the high σ–limit. In this case we have a quasi self–consistent solution, since the back reaction of the inertial plasma flow onto the guiding flux surface can indeed be neglected. Low σ–parameter solutions are shown in Figs. 6b,c,d. The physical wind flow is represented by that branch of the critical solution which starts with vanishing poloidal velocity at the injection radius of the field line $x_{\rm inj} = 0.01$ and then passes, with increasing velocity, the Alfvén point and the fast magnetosonic point. In the figure, those are defined by the points of intersection of the two solution branches.

Contrary to cold monopole configurations (e.g. Camenzind 1986) in our topology with a determined asymptotic jet radius the fast magnetosonic point moves inwards from infinity to a certain radius $x_{\rm FM}$.

In the high σ–limit, where magnetic forces dominate inertial forces, the narrowing of the flux tube beyond $x_{\rm FM}$ confines the plasma like in a magnetic bottle. The converging field lines decelerate the plasma. No steady physical solutions reaching the asymptotic radius were found. The deceleration takes place until the plasma velocity equals the magnetosonic velocity again, indicating possible shocks at this point. Stationarity will break down and instabilities will arise. Of course the derived asymptotic poloidal wind velocity in the high σ limit is relativistic, far from the observational value for protostellar jets and are applicable to neutron star jets (e.g. SS 433).

For low σ the plasma inertia is able to drive the wind to the asymptotic domain. The critical points move inwards. The situation is no more force–free. Figure 6d shows a wind solution with a terminal speed of several thousand km s^{-1}. The magnetization is $\sigma = 10^{-5}$. We expect that the terminal speed of a plasma flow with a magnetization $\sigma = 10^{-8}$ is of the order of the observed protostellar jet velocities. Again we like to note that the magnetization of the plasma may be different along different flux surfaces. This depends on the mass injection at the footpoints of the field lines. For a low density plasma flow, which may presumably take place along the innermost flux surfaces, the terminal speed may be indeed very high. The question of relativistic protostellar jet velocities was discussed e.g. by Kundt (1993).

Comparing the solutions to different σ–parameters, it can be seen that the high σ flows are predominantly accelerated in the region around the magnetosonic point, while acceleration in the low σ case occurs to a large part previous to the Alfvén point. The latter corresponds to a centrifugal acceleration due to rigid rotation of plasma and magnetosphere. This behavior is also mirrored in Fig. 6c where we show the toroidal velocity as a function of the radius. The toroidal velocity u_ϕ increases like $u_\phi \sim x$ until the Alfvén point. Here it decouples from a rigid rotation but still moves along the field lines.

The high σ solution demonstrates the general character of the acceleration process as a magnetically driven wind: The high magnetic energy reservoir allows for acceleration far beyond the Alfvén radius. It is possible to convert more Poynting flux into the kinetic energy of the low density plasma, and thus the asymptotic velocity drastically increases.

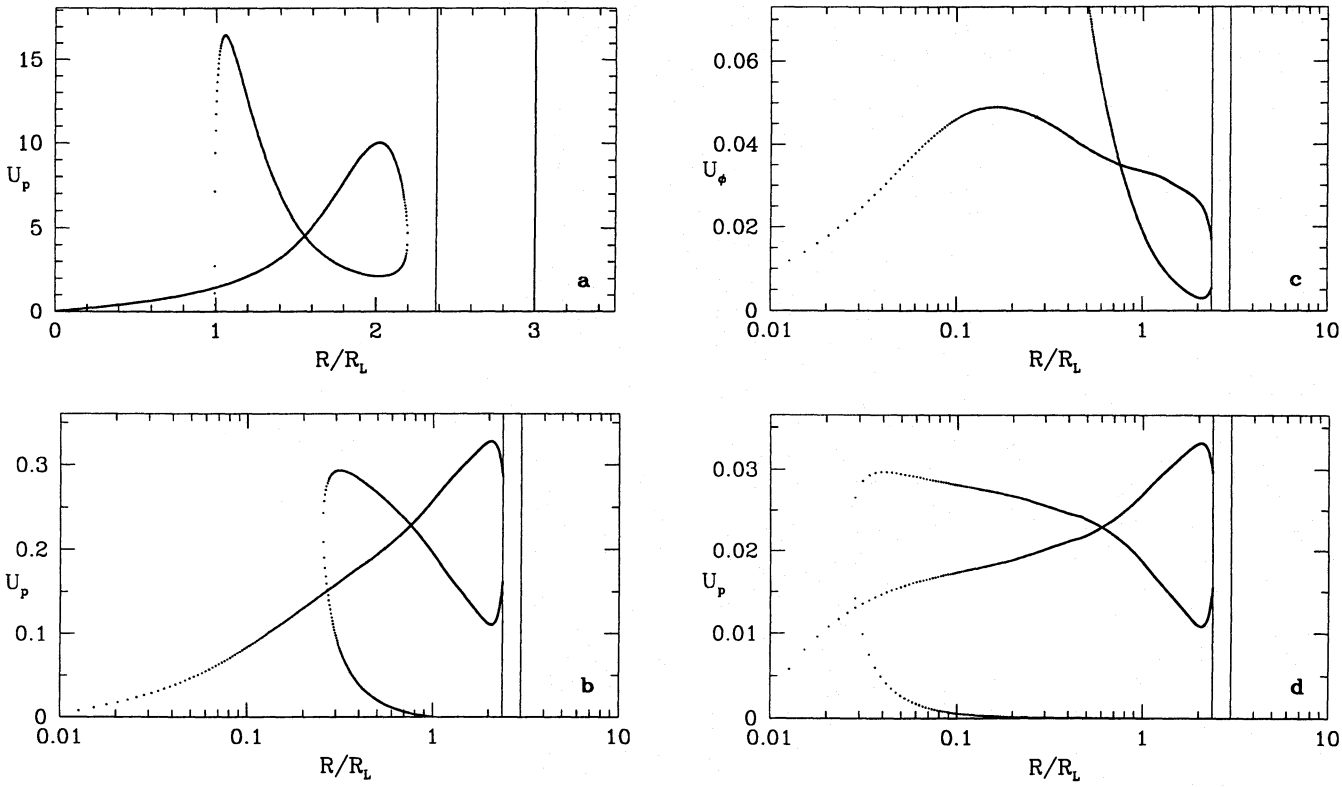

Fig. 6a–d. Solutions of the cold wind equation along the flux surface $\Psi = 0.733$. Poloidal $u_P(x)$ and toroidal $u_\phi(x)$ velocity, normalized to the speed of light. **a** $\sigma = 100$, **b, c** $\sigma = 0.01$, **d** $\sigma = 10^{-5}$. The vertical lines indicates the asymptotic radius of the flux surface $x_\infty = 2.377$ and the asymptotic jet radius $x_{\rm jet} = 3$. Alfvén and fast magnetosonic radii, $x_{\rm A}, x_{\rm FM}$: 0.994, 1.53 (**a**), 0.268, 0.76 (**b**), 0.029, 0.60 (**d**). Note the different scaling of the abscissæ

For a solution of the hot wind equation along flux surfaces similar to our configuration we refer to the results of Paatz & Camenzind (1994).

5.4. Model topology ARP

The results for the more ambitious model topology ARP are discriminated by the lack of a suitable starting configuration. When we start the iteration process with the solver that takes implicitly the Goldreich–Julian charge density into account, the procedure only converges in limited cases depending on the choice of $g_{\rm I}$ and $\Psi_{\rm cr}$. The poloidal current has to be small in the regime $x \gg x_{\rm in}$. Low $g_{\rm I}$ generally provide a weak current, while a set of high $g_{\rm I} \simeq 10^4$ and high $\Psi_{\rm cr} \simeq 0.4$ concentrates the current in the innermost part of the magnetosphere.

This current concentration may be compatible with a high mass accretion rate in the innermost part of the magnetosphere, in difference to the observed low mass flow in the jets. Indeed, using the current distribution Eq. (24), we found that the critical flux surface most far extending from the star is $\Psi = 0.4667$, which is exactly the surface bridging the inner disk boundary with the star.

However, for a weak poloidal current the regularity condition implies that *all* field lines have to pass the LC with vanishing slope. This seems to contradict the scenario of a collimated jet in the force–free limit. Figure 7 shows an example of a solution

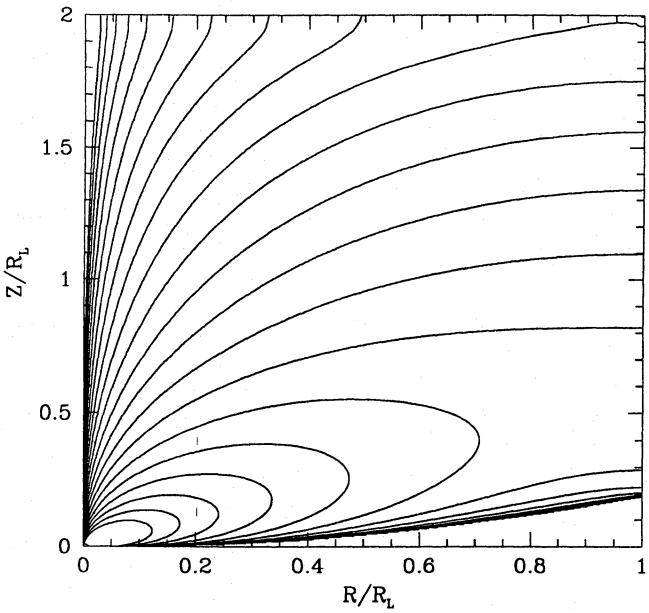

Fig. 7. Magnetic flux surface configuration in the regime within the LC in model ARP topology. Parameters: $g_{\rm I} = 100, \Psi_{\rm cr} = 0.41667$. Contour levels: $10^{-n}, n = 2, 8, 0.3$

to model ARP with a current distribution concentrated within a critical flux surface which originates at $x_c \simeq x_{in}$. Field lines crossing the LC will close in the outside regime, neglecting the upper jet boundary condition. Further, we were not able yet to solve the matching problem for this topology. This would require, as discussed above, a good estimate about the shape of the jet boundary as well as the current distribution along the flux surfaces.

6. Conclusion

In this work we presented numerical solutions of the relativistic 2D force balance equation for winds driven by strongly magnetized protostellar systems. We discussed two different models for a system containing a star surrounded by an accretion disk of different resistivity. The resulting field configuration allows simultaneously for wind outflow and mass accretion towards the central star. This is consistent with the observed link between the existence of outflows and the appearance of an accretion disk in the spectrum of these sources.

The open dipolar topology (model AMP) turns out to be most promising for the formation of jets. Even in the force–free limit, which neglects the inertia of the flowing wind, a fast collimation of a stellar dipolar magnetosphere towards a cylindrical jet structure with a finite asymptotic radius is possible. Many protostellar jets show opening angles of only a few degrees. These examples a well covered by jet solutions of nearly constant jet radius for $Z \geq R_L$. Newtonian jets extending beyond the light cylinder are therefore in agreement with the observed protostellar jet radii.

In these solutions, the flow is poorly collimated near the central star. We found an initial opening angle of the flow of 65°. This angle is determined by the regularity condition. The shape of the asymptotic jet boundary in our solution can be interpreted as given by pressure equilibrium with the ambient pressure distribution. Thus, we conclude that the initially free expanding jet is collimated by the pressure of the ambient molecular cloud.

The open dipolar topology also allows for jet collimation with moderate poloidal currents. The current strength of about 10^{11} A is in agreement with observational results of the jet bending and with equipartition arguments between the asymtotic jet and the ambient molecular cloud. A weak current corresponds to a flat current distribution. Since the mass flow per flux tube is directly correlated with the current distribution, these fast collimated, flat current distribution configurations would imply a homogeneous mass flow across the jet's diameter.

Using the force–free magnetic structures, we solved the wind equation along a certain surface near the edge of the jet for different magnetizations.

Solutions with a high magnetization are suitable to describe outflows driven by objects like SS 433, while protostellar jets with terminal velocities of 400 km s^{-1} may obtained for moderate magnetizations $\sigma \simeq 10^{-8}$. In this case, the Alfvén point moves inwards away from the LC to a region of several tens of stellar radii.

In the case of reversed field topologies (ARP) we obtain convergence only for a very low coupling constant g_I or for a current distribution concentrated near the innermost part of the magnetosphere. Although the last point is compatible with an accretion flow along the innermost field lines, the suitable regularity condition requires a vanishing slope of *all* field lines passing the LC. Therefore, a force–free jet extending beyond the LC is not possible.

Acknowledgements. This work was supported by the Deutsche Forschungsgemeinschaft (DFG). We are grateful to Prof. I. Appenzeller and Drs. S. Lamzin, R. Mundt and E. Guenther for discussions and comments.

Appendix A: numerical details

In this first part of the Appendix we point out some significant details of our numerical procedure.

Figure 8 shows an example of the numerical grid applied to a calculation simultaneously on the whole integration domain. The star–gap–disk system and the LC (optionally) are considered with a higher spatial resolution. For the scientific calculation we used a 64 x 64 finite element grid, respectively 12544 nodal points in the case of elements of the serendipity class. For a calculation on seperated domains we are able to apply this resolution for each integration domain.

In Fig. 9 we show numerical test solutions of our finite element solver (s. Sect. 4.2). Figure 9a exactly mirrors Michels (1973b) current–free solution of the classical pulsar equation derived with a totally different method. Figure 9b shows a monopol type configuration equivalent to the analytic solution Eq. (31). This solution, calculated from corresponding boundary conditions, is well behaved at the LC.

Appendix B: the matching problem

Due to the singularity in the GSS equation, the solution inside and outside the LC decouple and the regularity requirement provides a boundary condition at the LC. In general, global force–free solutions which extend beyond the LC, do not match up or show kinks at the LC. This matching problem is well known in the context of pulsar magnetospheres, but is not solved yet (Ingraham 1973; Pelizzari 1974; Sulkanen & Lovelace 1990; Michel 1991).

Obviously, it is hardly possible to solve the wind equation along such kinky flux surfaces and therefore, it became one of the essential points of this work to construct force–free magnetic field configurations, which are well behaved at the LC. In the following we describe the procedure which allowed us to gain well behaved solutions and discuss a possible physical interpretation.

In the case of the model topology AMP, the knowledge of the upper boundary condition, which represents the asymptotic jet, enables us to investigate independently the solutions inside and outside the LC. In Figure 10 we compare two solutions with the same shape of the jet boundary, but calculated seperately,

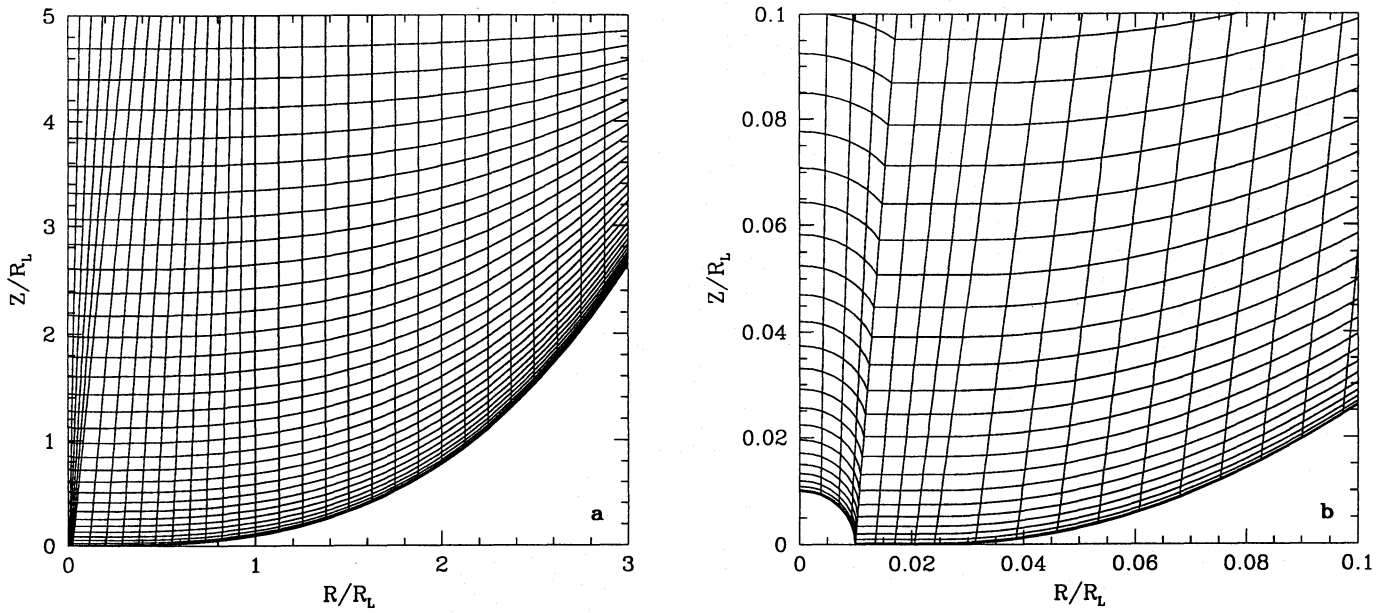

Fig. 8. a Example of a 32 x 32 grid applied to a calculation simultaneously on the whole integration domain. The disk height satisfies $z(x) \sim x^3$. **b** Subset of the innermost part of a full grid. Star, gap and disk are resolved

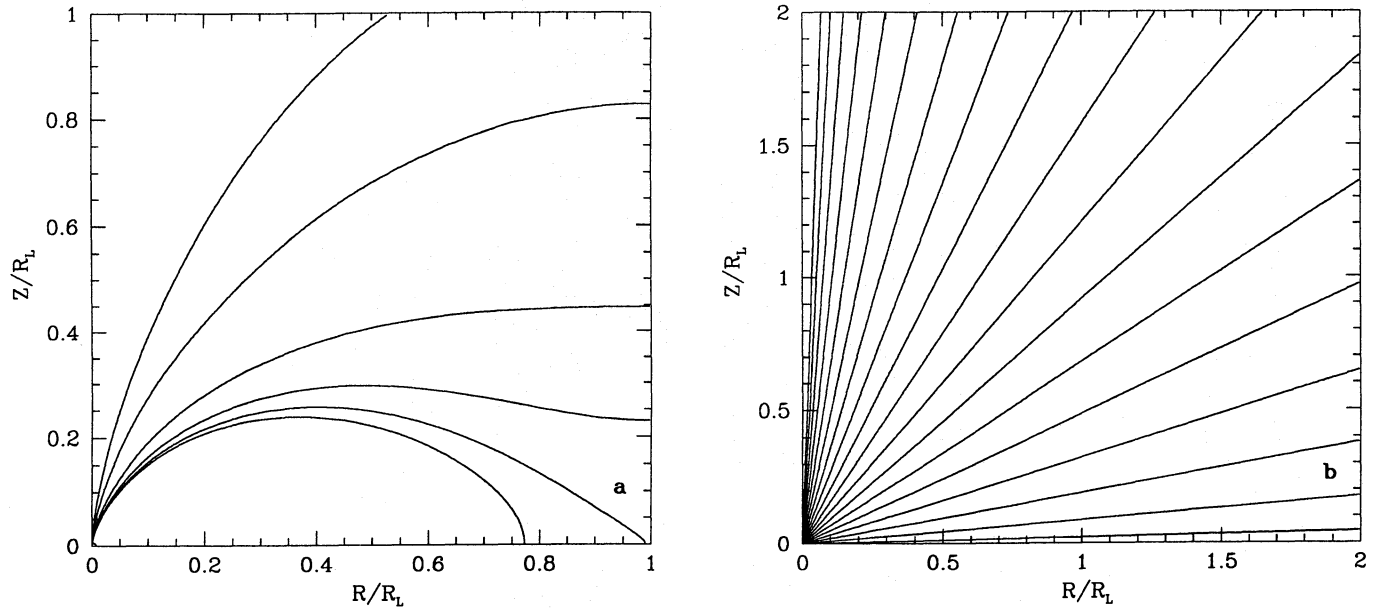

Fig. 9a and b. Numerical test solutions. **a** Dipolar field topology, contour levels: 0.15, 0.4, 1.0, 1.4, 1.592, 1.7. **b** Monopol type configuration, contour levels as in Fig. 3

respectively simultaneously on the inner and outer integration domain. We see that for any jet boundary, solution Fig. 10b is not steady at the LC, while solution Fig. 10a shows kinks at the LC.

From the work of Appl & Camenzind (1993a) we know that in the 1D asymptotic regime the solution $\Psi(x)$ for given $I(\Psi)$ is completely determined by the regularity condition. In particular, the jet radius $R_{\rm jet}$ is determined, since it is a parameter of the current distribution. But this argument cannot solely be applied for the jet *boundary* in a 2D regime, since $I(\Psi)$ is fixed by the asymtotic jet radius and is not anymore a function of the jet boundary $R_{\rm jet}(Z)$.

Therefore, we conjecture that in the 2D regime one may either adjust the shape of the jet boundary to a given current distribution, until the inner and outer solution match – or alternatively, to a given shape of the boundary, i.e. for prescribed outer boundary conditions, a corresponding current distribution can be found, but in general will have kinks. In other words:

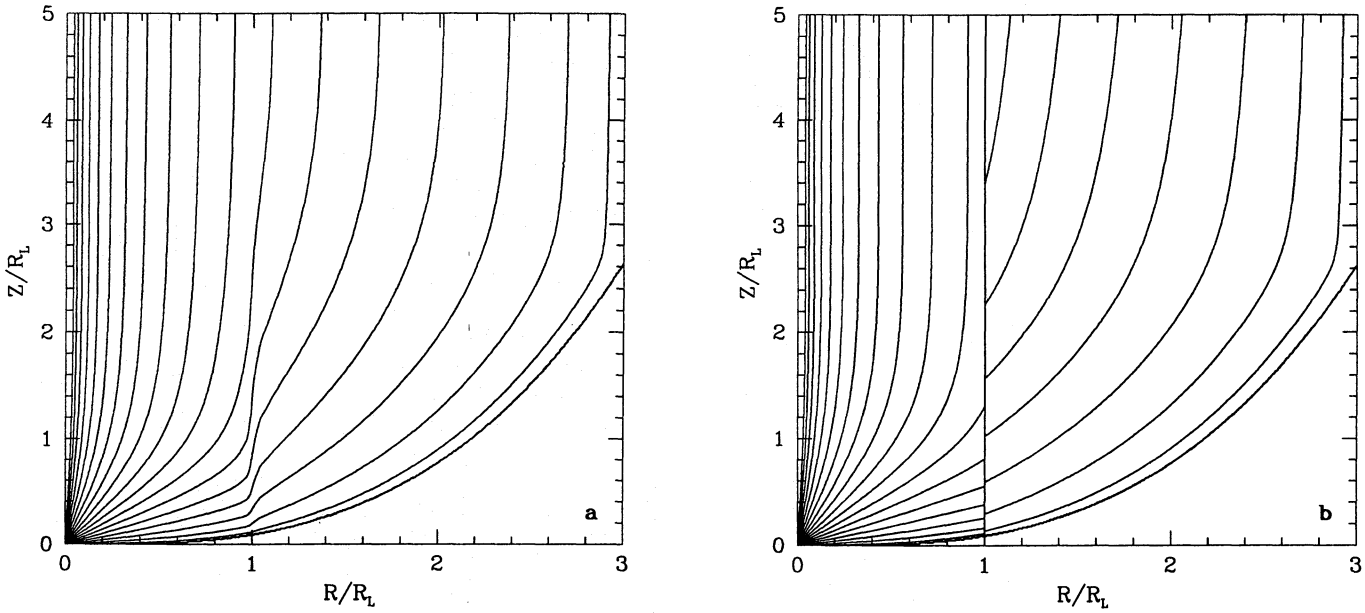

Fig. 10a and b. Magnetic flux distribution $\Psi(x, z)$ for model toplogy AMP for an ambiguous jet boundary. The solutions are calculated on the entire jet domain (**a**) and on seperate domains (**b**) inside and outside the LC. Parameters: b = 2.0, core radius a = 1.19, $x_{\rm jet}$ = 3.0, $g_{\rm I}$ = 1.28. Contour levels as in Fig. 3

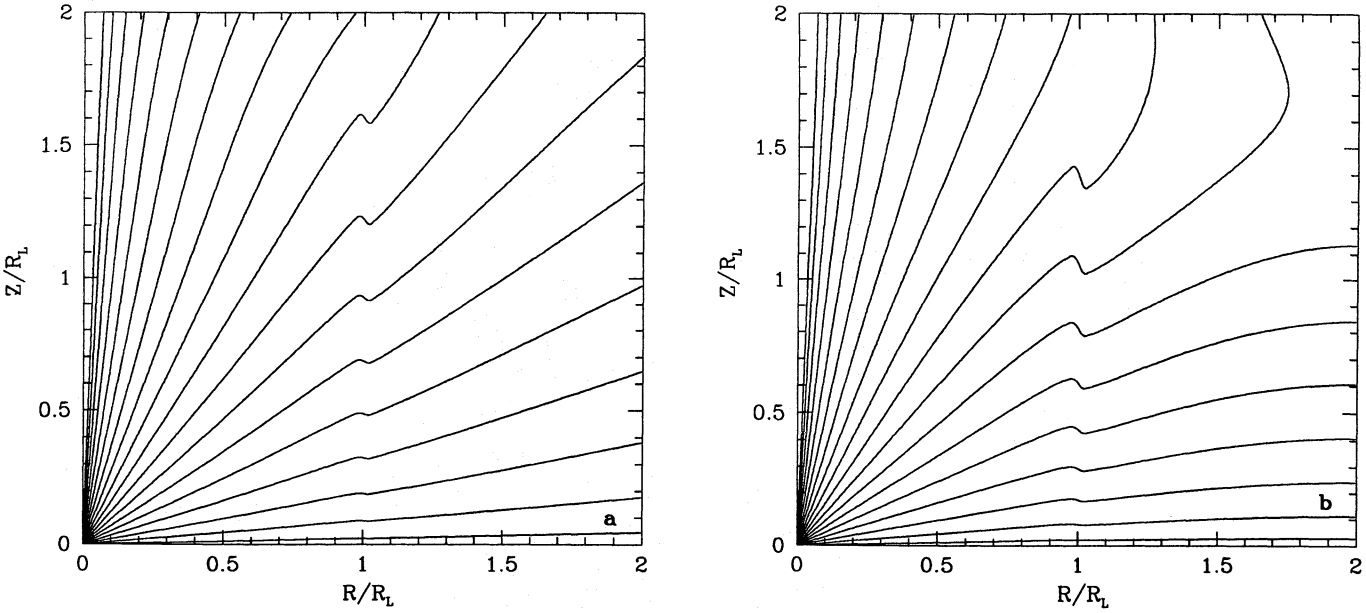

Fig. 11a and b. Influence of the current distribution or of the boundary conditions on the matching problem. Performation of the monopole type solution (Fig. 9b) by a alteration of the current strength by 10% (**a**) and the outer boundary condition from Dirichlet to homogeneous Neumann (**b**). Contour levels as in Fig. 9b

For a given current distribution, we have to match the shape of the jet boundary to the inner boundary condition. Or, for a fixed boundary, the solver gives the corresponding force–free distributions in Ψ and $I(\Psi)$.

As a demonstration of this boundary adjustment process, we show in Fig. 11 the performation of the analytic monopole type solution Eq. (31) (s. Fig. 9b): If we change the outer boundary condition from Dirichlet (satisfying a monopole solution) to homogeneous Neumann *or* vary the strength of the current, e.g. by a factor of 10%, we drastically influence the behavior of the solution around the LC.

For certain parameter sets b and $x_{\rm jet}$, i.e. for certain current distributions $I(\Psi)$, we found suitable jet boundaries providing AMP configurations with vanishing kinks at $R_{\rm L}$. Note that $I(\Psi)$ also influences the location of the jet boundary for $x \leq 1$ (Sect. 2.4).

To obtain a physical interpretation of the kinks we recall the interrelation between the magnetic pressure, $\simeq B_\phi^2$, the poloidal current, $I \simeq R B_\phi$, and the toroidal magnetic field. In this scheme the adjustment process corresponds to an adjustment of the pressure distribution in the domains inside and outside the LC, since a variation of the jet boundary corresponds to a variation of the jet volume and thus of the pressure.

An alternative explanation of the kinks may be the break down of the force–free assumption at the LC. Since $E_\perp \sim x B_\mathrm{P}$, currents $I_\perp$ could be expected, implying $I \neq I(\Psi)$. This would correspond to an additional current sheet. But, since the solution *has* to fulfill the force–free assumption by definition of Eq. (11), the flux surfaces, which follow the I = const. lines, will have kinks. From this point of view, the discontinuity of field lines in separatly calculated integration domains can be closed by an additional current at the LC, because it implies an additional magnetic flux via Ampère's law. In a calculation on the entire integration domain, the continuity requirement is intrinsically introduced.

The introduction of a singular current sheet was already discussed by Ingraham (1973), while Sulkanen & Lovelace (1990) claimed that such global solutions were unphysical and that the choice of $I(\Psi)$ has been specified without physical basis yet. However, we note that we selected $I(\Psi)$ from the physical asymptotic force equilibrium and that the fact that the poloidal current $I(\Psi)$ is a function of the flux surface is not violated by definition of our numerical technique.

References

Appenzeller, I., Mundt, R., 1989, A&AR, 1, 291
Appl, S., Camenzind, M., 1993a, A&A, 256, 354
Appl, S., Camenzind, M., 1993b, A&A, 270, 71
André, P., Montmerle, T., Stine, P.C., Feigelson, E.D., Klein, K.L., 1988, ApJ, 335, 940
André, P., Phillips, R.B., Lestrade, J.-F., Klein, K.L., 1991, ApJ, 376, 630
Beckwith, S.V.W., Sargent, A.I., Chini, R.S., Güsten, R., 1990, AJ, 99, 924
Bertout, C., 1989, ARA&A, 27, 351
Blandford, R.D., Payne, D.G., 1982, MNRAS, 199, 883 (BP)
Bouvier, J., 1990, AJ, 99, 946
Bouvier, J., Cabrit, S., Fernandez, M., Martin, E.L., Matthews, J.M., 1993, A&A, 272, 176
Camenzind, M., 1986, A&A, 162, 32
Camenzind, M., 1987, A&A, 184, 341
Camenzind, M., 1990, Magnetized disk–winds and the origin of bipolar outflows, in: Klare, G. (ed) Rev. Mod. Astron., 3, Springer, Heidelberg, p. 234 (CA)
Camenzind, M., Fendt, C., Paatz, G., 1994, in preparation (CFP)
Chandrasekhar, S., 1956, ApJ, 124, 232
Chiueh, T., Li., Z., Begelman, M.C., 1991, ApJ, 377, 462
D'Odorico, S., Oosterloo, T., Zwitter, T., Calvani, M., 1991, Nature, 353, 329
Edwards, S., Cabrit, S., Strom, S.E., Heyer, I., Strom, K., Anderson, E., 1987, ApJ, 321, 473
Fendt, C., 1994, PhD thesis, University of Heidelberg
Fendt, C., Camenzind, M., 1994, in preparation
Gosh, P., Lamb, F., 1978, ApJ, 223, L83
Hartmann, L.W., Raymond, J.C., 1989, ApJ, 337, 903
Heyvaerts, J., Norman, C.A., 1989, ApJ, 347, 1055
Ingraham, R.L., 1973, ApJ, 186, 625
Kazes, I., Crutcher, R.M., 1986, A&A, 164, 328
Kepner, J., Hartigan, P., Yang, C., Strom, S., 1993, ApJ, 15, L121
Königl, A., 1991, ApJ, 370, L39
Königl, A., Ruden, S.P., 1993, Origin of outflows and winds, in: Levy, E.H., Lunine, J.I. (eds) Protostars and Planets III, The University of Arizona Press, p. 641
Kundt, W., 1993, The bipolar outflow phenomenon, in: Errico, L., Vittone, A. (eds) Stellar Jets and Bipolar Outflows, Kluwer Academic Publishers, Dordrecht, p. 51
Lamb, F., 1989, Accretion by magnetic neutron stars, in: Ögelman, H., van den Heuvel, E.P.J. (eds) Timing Neutron Stars, Kluwer Academic Publishers, Dordrecht, p. 649
Michel, F.C., 1973a, ApJ, 180, L133
Michel, F.C., 1973b, ApJ, 180, 207
Michel, F.C., 1991, Theory of neutron star magnetospheres, The University of Chicago Press, Chicago
Montmerle, T., Feigelson, E.D., Bouvier, J., André, P., 1993, Magnetic fields, activity and circumstellar material around young stellar objects, in: Levy, E.H., Lunine, J.I. (eds) Protostars and Planets III, The University of Arizona Press, p. 689
Morse, J.H., Hartigan, P., Cecil, G., Heathcote, S., Raymond, J.C., 1992, ApJ, 399, 231
Morse, J.H., Heathcote, S., Cecil, G., Hartigan, P., Raymond, J.C., 1993, ApJ, 410, 764
Mundt, R., Brugel, E.W., Bührke, T., 1987, ApJ, 319, 275
Mundt, R., Ray, T.P., Bührke, T., Raga, A.C., Solf, J., 1990, A&A, 232, 37
Neukirch, T., 1993, A&A, 274, 319
Paatz, G., Camenzind, M., 1994, submitted to A&A
Pelizzari. M.A., 1974, M.S. Thesis, Rice University
Pelletier, G., Pudritz, R., 1992, ApJ, 394, 117
Pudritz, R., Norman, C.A., 1983, ApJ, 274, 677 (PN)
Reipurth, B., 1989, A&A, 220, 249
Safier, P.N., 1993, ApJ, 408, 115
Sakurai, N.I., 1985, A&A, 152, 121
Sakurai, N.I., 1987, Publ. astr. Soc. Japan, 39, 821
Scharlemann, E.T., Wagoner, R.V., 1973, ApJ, 182, 951
Schwarz, H.R., 1984, Methode der finiten Elemente, Teubner Studienbücher, Stuttgart
Solf, J., Böhm, K.H., 1993, ApJ, 410, L31
Sulkanen, M.E., Lovelace, V.E., 1990, ApJ, 350, 732

This article was processed by the author using Springer-Verlag LaTeX A&A style file version 3.